A High Order Nonlinear Adaptive Observer for PMSM Speed-Flux Transformation Model: A PMSM Sensorless Control Scheme

Siyuan Liu, *Graduate Student Member, IEEE*, Ling Liu, *Member, IEEE*, Qilian Lin, *Student Member, IEEE*, Dongsong Jin, *Student Member, IEEE*, and Deliang Liang, *Senior Member, IEEE*

***Abstract*—This article presents a novel speed-flux transformation model, derived from the traditional active flux model of permanent magnet synchronous motor, which features a known regression term of speed. This advancement achieves nonlinear parameterization of motor speed, enabling the construction of a speed adaptive observer. Then, a high order nonlinear adaptive (HONA) observer is developed by adopting the proposed model, which employs a nonlinear parameter updating law and high order sliding mode correction terms for error estimators, thereby enhancing the system's dynamic response. Due to the known regression term nature of the proposed model, the adaptive observer ensures stability at near-zero speeds, leading to superior performance in low-speed and reversal scenarios. After rigorously proving the observer's stability, a detailed tuning guide for parameters is provided. The effectiveness of the HONA observer is validated through both numerical and experimental works.**

***Index Terms*—Nonlinear adaptive observer, nonlinear parametrization, permanent magnet synchronous motor (PMSM), sensorless control.**

I. Introduction

In recent years, the topic of sensorless control has attracted significant interest from researchers. Since it relief the need for speed sensors in motor control, which can lead to increased costs and reduced reliability [1], [2], [3], [4], [5]. Among various driving objects, permanent magnet synchronous motors (PMSMs) have emerged prominently in sensorless drive research due to their high efficiency and high power density characteristics. In this context, both motor speed and position information play crucial roles in closed-loop control. For sensorless control techniques, they can generally be divided into two categories: saliency based and model based methods [1], [2], [3]. As reported in [1], conventional model based sensorless control strategies rely on extended electromotive force (EMF) model [2], active flux model [3], and so forth. For the traditional model based methods, the basic concept is to set the states to be observed (e.g., EMF and active flux) as a disturbance, then apply a disturbance observer to estimate it. Finally, calculate the angle and corresponding speed based on the observed values [4]. However, this method incorporates uncertainties from the dynamics within the observed estimated values. Therefore, as mentioned in [5], a common approach to improve observational accuracy is to extend the quantities to be observed to higher order states. Constrained by inherent limitations of the models, these method based strategies are typically suitable for high-speed operation stages, making it challenging to achieve satisfactory performance across a wide speed range [6], [7]. Therefore, to enhance the stability of motor operation at low speeds, it motivates us to design a globally stable adaptive observer.

However, it fails to design a globally stable speed adaptive observer through traditional motor models (e.g., EMF model and active flux model). As discussed in [8] and [9], the primary reason is that the motor speed regression term is unknown. This implies that the speed regression term includes unknown states, such as EMF and active flux, which cannot be directly measured. As the speed approaches zero, these states also tend to zero, leading to an increase in estimation error [10]. This suggests to achieve global stability for the speed adaptive observer, one feasible approach is to construct a model with known regression terms for motor speed through nonlinear parameterization. Therefore, this article adopts the traditional PMSM active flux model and applies nonlinear parameterization to the motor speed to achieve known regression term of speed. This implies that the speed regression terms only include directly measurable information, such as voltage and current, thereby providing a foundational model for constructing a globally stable speed adaptive observer.

In motor states observation, many attempts have been made in applying adaptive observers because of its advantage of adaptive correction that follows the motor states, such as the sliding mode observer (SMO) with adaptive coefficients designed in [11]. However, due to inherent limitations of the traditional EMF model, it still constraints at low speeds. In [12], the motor speed is treated as a parameter, then a globally stable adaptive

Received 31 December 2024; revised 17 March 2025; accepted 12 April 2025. Date of publication 16 April 2025; date of current version 26 May 2025. This work was supported by the National Natural Science Foundation of China under Grant 51977173. Recommended for publication by Associate Editor K.-B. Park. *(Corresponding author: Ling Liu.)*

The authors are with the State Key Laboratory of Electrical Insulation and Power Equipment, School of Electrical Engineering, Xi'an Jiaotong University, Xi'an 710000, China (e-mail: 3121304035@stu.xjtu.edu.cn; liul@mail.xjtu.edu.cn; lql971022@stu.xjtu.edu.cn; jindongsong@stu.xjtu.edu.cn; dlliang@mail.xjtu.edu.cn).

Color versions of one or more figures in this article are available at https://doi.org/10.1109/TPEL.2025.3561555.

Digital Object Identifier 10.1109/TPEL.2025.3561555

observer for induction motors was designed. But like most adaptive observers to observe states and parameters simultaneously (e.g., [13] and [14]), their parameter updating law is set to be linear and the convergence rates are asymptotic or exponential. Besides, liner observer is proved to be falls into the typical form of high gain observers, which fails to achieve satisfactory dynamic performance and resistance to high frequency noise simultaneously [15].

Therefore, to enhance the dynamic response of the observer, a potential approach is to construct the correction term as nonlinear to form a nonlinear observer for observing the electrical states (e.g., EMF and active flux) of the motor [17], [18], [19]. Another approach involves using the observed electrical states to construct a nonlinear extended state observer (ESO), which enhances the dynamic response of the motor's mechanical states (e.g., rotor position and speed) [10], [20], [21]. Among nonlinear observers, it is natural to construct SMO since its robustness and easy to apply. SMO is a typical class nonlinear observer, which introduces sign function into the correction term, but since the inherent limitations of conventional models, it fails to achieve global stable [10]. Therefore, conventional SMO struggles for the low speed performance [22].

To address the aforementioned issues, this article conduct a kind of speed-flux transformation to the traditional PMSM active flux model and proposes a high-order nonlinear adaptive (HONA) observer through this model. The observer incorporates a nonlinear parameter updating law and designs the correction term for the estimation error dynamics in the form of a high order sliding mode. Mathematical proofs are provided to demonstrate that the proposed HONA observer can achieve finite-time input-to-state stability (FT-ISS) of the state estimation error with respect to the parameter identification error.

The rest of this article is organized as follows. The problem statement is arranged in Section II. The high order nonlinear adaptive observer is designed in Section III. The stability analysis and tuning guideline are also conducted in this section. Then, some numerical results are shown in Section IV accompanied by experimental results in Section V. Finally, Section VI concludes this article.

II. Problem Statement

This section aims to discuss the issues existing in adaptive observers for speed estimation under traditional flux models. Due to the presence of unknown regressor in the dynamic equations, adaptive observers are unable to achieve global stability.

A. Modeling of Conventional Active Flux Model

According to [3], define $\alpha\beta$-axis active flux $\boldsymbol{\psi}_a = [\psi_{a\alpha} \quad \psi_{a\beta}]^T$ of PMSM as $\boldsymbol{\psi}_a = \boldsymbol{\psi}_s - L_q\boldsymbol{i}$. Then, the conventional active flux model under $\alpha\beta$ frame can be written as

$$p\boldsymbol{i} = \frac{1}{L_q}\boldsymbol{u} - \frac{R_s}{L_q}\boldsymbol{i} - \omega\boldsymbol{J}\frac{\boldsymbol{\psi}_a}{L_q} \tag{1a}$$

$$p\boldsymbol{\psi}_a = \omega\boldsymbol{J}\boldsymbol{\psi}_a + \boldsymbol{w}(t) \tag{1b}$$

where $\boldsymbol{\psi}_s = \int(\boldsymbol{u} - R_s\boldsymbol{i})dt$ denotes stator flux; $p = d/dt$ denotes differential operator; $\boldsymbol{u} = [u_\alpha \quad u_\beta]^T$ and $\boldsymbol{i} = [i_\alpha \quad i_\beta]^T$ denote stator voltage and current under $\alpha\beta$-axis, respectively, $\boldsymbol{u}$ and $\boldsymbol{i}$ are also known as the input of the system; R_s is the stator resistance; L_q is the stator inductance under q-axis; $\boldsymbol{J} = \begin{bmatrix} 0 & -1 \\ 1 & 0 \end{bmatrix}$; ω is the rotor electrical angular velocity; $\boldsymbol{w}(t) = [w_\alpha(t) \quad w_\beta(t)]^T$ is the q-axis transient disturbance.

Reformulate (1) into the form of classical uncertain nonlinear systems as

$$p\boldsymbol{x} = \boldsymbol{A}\boldsymbol{x} + \boldsymbol{\phi}(\boldsymbol{y}, \boldsymbol{u}_{\text{in}}) + \boldsymbol{G}(t, \boldsymbol{y}, \boldsymbol{u}_{\text{in}})\vartheta + \boldsymbol{D}\boldsymbol{w}(t) \tag{2}$$

where

$$\boldsymbol{x} = \begin{bmatrix} \boldsymbol{i} \\ \boldsymbol{\psi}_a \end{bmatrix}, \boldsymbol{A} = \begin{bmatrix} -R_s/L_q & -\omega\boldsymbol{J}/L_q \\ 0 & \omega\boldsymbol{J} \end{bmatrix}, \vartheta = \omega, \tag{3a}$$

$$\boldsymbol{\phi} = \begin{bmatrix} \frac{1}{L_q}\boldsymbol{u} \\ 0 \end{bmatrix}, \boldsymbol{G} = \begin{bmatrix} -\boldsymbol{J}\boldsymbol{\psi}_a/L_q \\ \boldsymbol{J}\boldsymbol{\psi}_a \end{bmatrix}, \boldsymbol{D} = \begin{bmatrix} 0 \\ \boldsymbol{I} \end{bmatrix}. \tag{3b}$$

Here, $\boldsymbol{y}$ and $\boldsymbol{u}_{\text{in}}$ denote the input and output of the system, respectively; ϑ denotes the system parameter; $\boldsymbol{G}$ represents the regression term. It can be observed that $\boldsymbol{G}$ includes unmeasurable component $\boldsymbol{\psi}_a$, which is known as unknown regressor. As discussed in [12], systems with unknown regressor cannot establish globally stable adaptive observers.

B. Speed-Flux Transformation

To address the issue of unknown regressor, define

$$\begin{cases} \boldsymbol{\psi}_\mu = L_q\boldsymbol{i} \\ \boldsymbol{\varpi}_\psi = -\omega\boldsymbol{J}\boldsymbol{\psi}_s. \end{cases} \tag{4}$$

Then, the PMSM active flux model (1) can be transformed as

$$\begin{aligned} p\boldsymbol{\psi}_\mu &= \boldsymbol{u} - R_s\boldsymbol{i} - \omega\boldsymbol{J}(\boldsymbol{\psi}_a + L_q\boldsymbol{i}) + \omega\boldsymbol{J}L_q\boldsymbol{i} \\ &= \boldsymbol{u} - R_s\boldsymbol{i} + \boldsymbol{\varpi}_\psi + \omega\boldsymbol{J}L_q\boldsymbol{i} \end{aligned} \tag{5a}$$

$$p\boldsymbol{\varpi}_\psi = -\omega\boldsymbol{J}(\boldsymbol{u} - R_s\boldsymbol{i}) + \boldsymbol{w}(t). \tag{5b}$$

For system (5), the input is stator voltage and current $\boldsymbol{u}$, $\boldsymbol{i}$ with the output

$$\boldsymbol{y} = \boldsymbol{C}\boldsymbol{x} \tag{6}$$

where $\boldsymbol{C} = [\boldsymbol{I} \quad 0]$.

Rewrite (5) into the form of (2), then

$$\boldsymbol{x} = \begin{bmatrix} \boldsymbol{\psi}_\mu \\ \boldsymbol{\varpi}_\psi \end{bmatrix}, \boldsymbol{A} = \begin{bmatrix} 0 & \boldsymbol{I} \\ 0 & 0 \end{bmatrix}, \vartheta = \omega, \boldsymbol{D} = \begin{bmatrix} 0 \\ \boldsymbol{I} \end{bmatrix} \tag{7a}$$

$$\boldsymbol{\phi} = \begin{bmatrix} \boldsymbol{u} - R_s\boldsymbol{i} \\ 0 \end{bmatrix}, \boldsymbol{G} = \begin{bmatrix} \boldsymbol{J}L_q\boldsymbol{i} \\ -\boldsymbol{J}(\boldsymbol{u} - R_s\boldsymbol{i}) \end{bmatrix}. \tag{7b}$$

It should be noted that in this case, the regression term $\boldsymbol{G}$ contains only directly measurable stator voltage and current. This implies that the issue of unknown regression terms in traditional active flux model has been transformed into a nonlinear parameterization problem with known regression term. As discussed in [9], the mathematical model with known regression term can release the issue of failed globally stable adaptive observer designation.

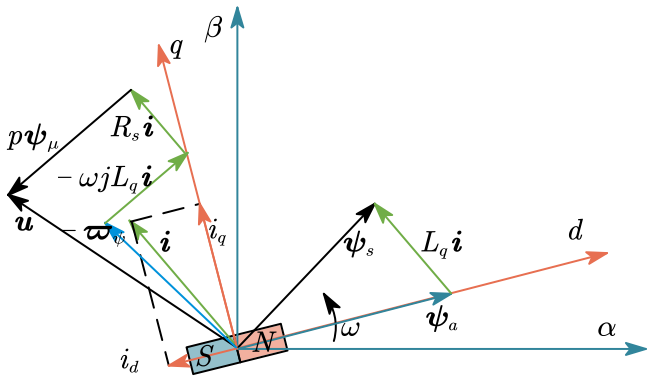

Fig. 1. Vector diagram of speed-flux transformation.

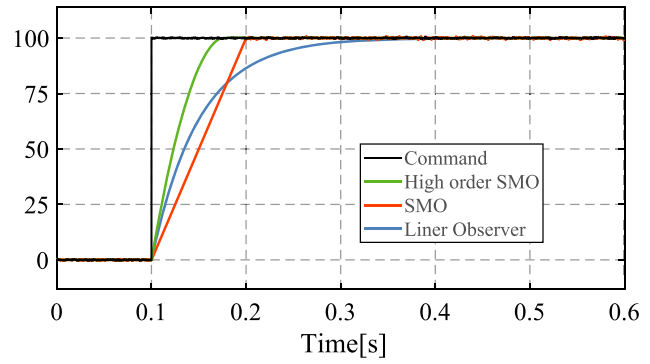

Fig. 2. Dynamic response comparison of different observers.

Besides, due to the relative degree between $\boldsymbol{w}(t)$ and ψ_μ being greater than 1, this term is often neglected in the design of most observers, prompting the development of an observer in this article that takes this disturbance into account.

III. High Order Nonlinear Adaptive Observer

Fig. 2 presents a set of comparative simulation results, which demonstrates the dynamic performance of SMOs, which are typical nonlinear observers, compared to linear observer, motivating us to design high order nonlinear observer to achieve better steady-state and dynamic performance. It can be observed from Fig. 2 that although SMO enhances dynamic response compared to liner observer, it inevitably introduces chattering effects. Conversely, high order SMO can mitigate this issue.

Meanwhile, to address the issue of q-axis transient disturbance $\boldsymbol{w}(t)$ relative degree not being 1, this section design a nonlinear parameterized high-order adaptive observer for (5). The nonlinear observer ensures FT-ISS of the the state estimation error with respect to the parameter identification error.

A. Adaptive Observer Design Procession

For system (5)–(7), let us design the nonlinear adaptive observer as

$$p\boldsymbol{\Omega} = (\boldsymbol{A}-\boldsymbol{LC})\,\boldsymbol{\Omega} + \boldsymbol{G}(t,\boldsymbol{y},\boldsymbol{u}_{in}) \tag{8a}$$

$$p\hat{\vartheta} = \boldsymbol{\tau}\boldsymbol{\Omega}^T\boldsymbol{C}^T\langle \boldsymbol{y}-\boldsymbol{C}\hat{\boldsymbol{x}}\rangle^\alpha \tag{8b}$$

$$\hat{\boldsymbol{x}} = \boldsymbol{\gamma} + \boldsymbol{T}^{-1}\boldsymbol{\eta} \tag{8c}$$

$$p\boldsymbol{\gamma} = \boldsymbol{A}\boldsymbol{\gamma} + \boldsymbol{\phi}(\boldsymbol{y},\boldsymbol{u}_{in}) + \boldsymbol{G}(t,\boldsymbol{y},\boldsymbol{u}_{in})\,\hat{\vartheta} + \boldsymbol{L}(\boldsymbol{y}-\boldsymbol{C}\boldsymbol{\gamma}) + \boldsymbol{\Omega}p\hat{\vartheta} \tag{8d}$$

$$p\boldsymbol{\eta} = \boldsymbol{B}\boldsymbol{\eta} + \boldsymbol{a}(\boldsymbol{y}-\boldsymbol{C}\boldsymbol{\gamma}) + \boldsymbol{\chi}(\eta_1,\boldsymbol{y}-\boldsymbol{C}\boldsymbol{\gamma}) \tag{8e}$$

where $\boldsymbol{\Omega}$ is an auxiliary martix; $\boldsymbol{L}\in\mathbb{R}^4$ is the gain vector, the selection of which should ensure that $(\boldsymbol{A}-\boldsymbol{LC})$ is Hurwitz; $\boldsymbol{\tau}$ is the gain matrix satisfy $\boldsymbol{\tau}=\boldsymbol{\tau}^T>0$; notation $\hat{}$ denotes an estimator of the real states and parameter; the transformation matrix $\boldsymbol{T}\in\mathbb{R}^{4\times4}$ satisfying

$$\boldsymbol{T}^{-1} = \begin{bmatrix}(\boldsymbol{A}-\boldsymbol{LC})\,\boldsymbol{\xi} & \boldsymbol{\xi}\end{bmatrix}$$

where $\boldsymbol{\xi}$ is given by $\boldsymbol{\xi}=\boldsymbol{\mathcal{O}}^{-1}\boldsymbol{h}$, $\boldsymbol{\mathcal{O}}$ is the observability matrix of the pair $(\boldsymbol{A}-\boldsymbol{LC},\boldsymbol{C})$, and $\boldsymbol{h}=[0\quad \boldsymbol{I}]^T$; $\boldsymbol{\gamma}\in\mathbb{R}^4$ is the Luenberger state estimation; vector $\boldsymbol{\eta}\in\mathbb{R}^4$ stands for an estimator of the error between $\boldsymbol{x}$ and $\boldsymbol{\gamma}$. The operator $\langle\cdot\rangle^\alpha$ is defined as $\langle\cdot\rangle^\alpha = |\cdot|^\alpha\mathrm{sign}(\cdot)$.

Remark 1: Note that (8b) is the nonlinear parameterized dynamic equation, whose characteristics are determined by α. When $\alpha=1$, it is a linear high-gain observer; while $\alpha\in(0,1)$, it exhibits continuous nonlinear characteristic; if $\alpha=0$, a discontinuous observer is obtained.

Then the vector form representation of $\boldsymbol{\Omega}\in\mathbb{R}^4$ is as follows:

$$\begin{aligned} p\boldsymbol{\Omega} &= p\begin{bmatrix}\boldsymbol{\Omega}_1\\ \boldsymbol{\Omega}_2\end{bmatrix} \\ &= (\boldsymbol{A}-\boldsymbol{LC})\begin{bmatrix}\boldsymbol{\Omega}_1\\ \boldsymbol{\Omega}_2\end{bmatrix} + \begin{bmatrix}\boldsymbol{J}L_q\boldsymbol{i}\\ -\boldsymbol{J}(\boldsymbol{u}-R_s\boldsymbol{i})\end{bmatrix} \end{aligned} \tag{9}$$

where $\boldsymbol{\Omega}=[\boldsymbol{\Omega}_1\quad\boldsymbol{\Omega}_2]^T$ and $\boldsymbol{\Omega}_1,\boldsymbol{\Omega}_2\in\mathbb{R}^2$.

Expressing the parameter updating dynamics in vector form, we have

$$\begin{aligned} p\hat{\vartheta} = p\hat{\omega} &= \boldsymbol{\tau}\begin{bmatrix}\boldsymbol{\Omega}_1^T & \boldsymbol{\Omega}_2{}^T\end{bmatrix}\begin{bmatrix}\boldsymbol{I}\\ 0\end{bmatrix}\langle\boldsymbol{y}-\boldsymbol{C}\hat{\boldsymbol{x}}\rangle^\alpha \\ &= \boldsymbol{\tau}\boldsymbol{\Omega}_1{}^T\langle\psi_\mu-\hat{\psi}_\mu\rangle^\alpha. \end{aligned} \tag{10}$$

The Luenberger state estimation of system states $\boldsymbol{x}$ can be expressed in the following manner:

$$\begin{aligned} p\boldsymbol{\gamma} = &\begin{bmatrix}0 & \boldsymbol{I}\\ 0 & 0\end{bmatrix}\begin{bmatrix}\boldsymbol{\gamma}_1\\ \boldsymbol{\gamma}_2\end{bmatrix} + \begin{bmatrix}\boldsymbol{u}-R_s\boldsymbol{i}\\ 0\end{bmatrix} \\ &+\begin{bmatrix}\boldsymbol{J}L_q\boldsymbol{i}\\ -\boldsymbol{J}(\boldsymbol{u}-R_s\boldsymbol{i})\end{bmatrix}\hat{\omega} + \boldsymbol{L}(\psi_\mu-\boldsymbol{\gamma}_1) + \boldsymbol{\Omega}p\hat{\omega} \end{aligned} \tag{11}$$

where $\boldsymbol{\gamma}=[\boldsymbol{\gamma}_1\quad\boldsymbol{\gamma}_2]^T$ and $\boldsymbol{\gamma}_1,\boldsymbol{\gamma}_2\in\mathbb{R}^2$.

The observer outputted estimated states $\hat{\boldsymbol{x}}$ is

$$\hat{\boldsymbol{x}} = \begin{bmatrix}\hat{\psi}_\mu\\ \hat{\varpi}_\psi\end{bmatrix} = \begin{bmatrix}\boldsymbol{\gamma}_1\\ \boldsymbol{\gamma}_2\end{bmatrix} + \boldsymbol{T}^{-1}\begin{bmatrix}\boldsymbol{\eta}_1\\ \boldsymbol{\eta}_2\end{bmatrix} \tag{12}$$

where $\boldsymbol{\eta}=[\boldsymbol{\eta}_1\quad\boldsymbol{\eta}_2]^T$ and $\boldsymbol{\eta}_1,\boldsymbol{\eta}_2\in\mathbb{R}^2$.

In (8e), the matrix $\boldsymbol{B}\in\mathbb{R}^{4\times4}$ and $\boldsymbol{a}\in\mathbb{R}^{4\times2}$ are given as

$$\boldsymbol{B} = \begin{bmatrix}0 & \boldsymbol{I}\\ 0 & 0\end{bmatrix}, \boldsymbol{a} = \begin{bmatrix}a_1\boldsymbol{I}\\ a_2\boldsymbol{I}\end{bmatrix}$$

where $a_i, i=1,2$ are the coefficients of the characteristic polynomial of the matrix $(\boldsymbol{A}-\boldsymbol{LC})$. The nonlinear injection

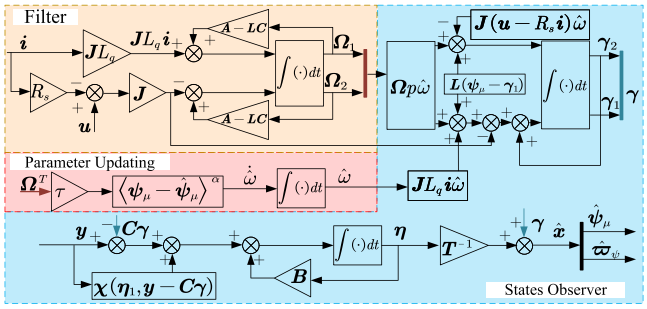

Fig. 3. Implementation block diagram of HONA observer (8).

$\boldsymbol{\chi}(\boldsymbol{\eta}_1, \boldsymbol{y}-\boldsymbol{C\gamma})$ of (8e) is designed as

$$\begin{aligned}\boldsymbol{\chi}\left(\boldsymbol{\eta}_1, \boldsymbol{y}-\boldsymbol{C\gamma}\right) &= \begin{bmatrix} k_1\langle(\boldsymbol{y}-\boldsymbol{C\gamma})-\boldsymbol{\eta}_1\rangle^{\frac{1}{2}} \\ k_2\langle(\boldsymbol{y}-\boldsymbol{C\gamma})-\boldsymbol{\eta}_1\rangle^{0}\end{bmatrix} \\ &= \begin{bmatrix} k_1\langle\left(\boldsymbol{\psi}_\mu-\boldsymbol{\gamma}_1\right)-\boldsymbol{\eta}_1\rangle^{\frac{1}{2}} \\ k_2\langle\left(\boldsymbol{\psi}_\mu-\boldsymbol{\gamma}_1\right)-\boldsymbol{\eta}_1\rangle^{0}\end{bmatrix}\end{aligned} \tag{13}$$

where $k_i, i=1,2$ are some positive gains. Fig. 3 shows the block diagram of HONA observer (8).

Besides, since we have already designed the speed parameter updating law (10), by adopting a certain approach, it is possible to observe the load torque, thereby enhancing the robustness of sensorless control scheme to the load. Now, let us design a specialized cascaded ESO to extend the estimated load torque as a first-order dynamic, thus achieving load torque observation without affecting speed observation.

Recalling the mechanical dynamics of PMSM

$$\begin{cases} p\theta = \omega \\ p\omega = \left(\frac{3}{2}n_{pp}\psi_{\text{active}}i_q\right)\frac{n_{pp}}{J_s} - T_L. \end{cases} \tag{14}$$

Remark 2: It should be noted that for the convenience of following analysis, there exists a coefficient J_s/n_{pp} between the actual load torque and the load torque T_L in the dynamic (14).

Conventional ESO will introduce estimated load torque $\hat{T}_L$ in the parameter updating law, leading to coupling issues that affect speed estimation; alternatively introducing additional estimated speed fitting quantities, which would inevitably lead to increased system complexity and reduced estimation accuracy. To conduct load torque observation, a candidate observer employing a special cascade form is presented in [16]. The primary feature of the ESO proposed in [16] is that the output of the lower order dynamics serves as the input for the higher order dynamics, allowing it to be regarded as a series of individual first-order ESOs. For interested readers, the detailed stability analysis of such observer has been provided in [16]. Then, we design a specialized cascade ESO as follows:

$$p\hat{T}_L = \frac{g\left(\bar{T}_L\right)}{\tau_T} \tag{15}$$

where $g(x):\mathbb{R}\to\mathbb{R}$ is an odd continuous function; τ_T is small enough positive constant; $\bar{T}_L$ is the error yields

$$\begin{aligned}\bar{T}_L &= p\hat{\omega} - \bar{K}_{i_q} + \hat{T}_L \\ &= \boldsymbol{\tau}{\boldsymbol{\Omega}_1}^T\langle\boldsymbol{\psi}_\mu - \hat{\boldsymbol{\psi}}_\mu\rangle^\alpha - \bar{K}_{i_q} + \hat{T}_L\end{aligned} \tag{16}$$

where $\bar{K}_{i_q} = (\frac{3}{2}n_{pp}\psi_{\text{active}}i_q)$.

B. Stability Analysis

For the convenience of the stability analysis, the adaptive observer (8) can effectively be divided into two parts: the parameter updating law (8b) and the high order nonlinear states observer (8d) and (8e). Therefore, their stability will be analyzed separately in the following. For the convenience of describe, define the operator $\epsilon_{\min}(\boldsymbol{A}) = \sqrt{\lambda_{\min}(\boldsymbol{A}^T\boldsymbol{A})}, \epsilon_{\max}(\boldsymbol{A}) = \sqrt{\lambda_{\max}(\boldsymbol{A}^T\boldsymbol{A})}$.

1) Parameter Updating Law: First, the estimation error of the parameter is defined as $\tilde{\vartheta} = \hat{\vartheta} - \vartheta$. For system (5), the parameter ϑ is rotor speed ω, then the estimation error of the rotor speed is $\tilde{\omega} = \hat{\omega} - \omega$. The dynamic of $\tilde{\omega}$ yields

$$\dot{\tilde{\omega}} = \boldsymbol{\tau}{\boldsymbol{\Omega}_1}^T\langle\boldsymbol{\psi}_\mu - \hat{\boldsymbol{\psi}}_\mu\rangle^\alpha. \tag{17}$$

The following lemma gives the FT-ISS of (17) with respect to the input $\boldsymbol{\xi} = \boldsymbol{T\delta} - \boldsymbol{\eta}$, where $\boldsymbol{\delta} = \boldsymbol{x} - \boldsymbol{\gamma} + \boldsymbol{\Omega}\tilde{\omega}$, for $\alpha\in(0,1)$ and $\alpha = 0$.

Lemma 1 (See [23]): Let $0 < \varrho_{\min} < \epsilon_{\min}(\boldsymbol{C\Omega}(t))$ for all $t>0$ and $||\boldsymbol{C\Omega}||_\infty < \varrho_{\max} < +\infty$. Then, for $\alpha\in(0,1)$, the dynamic (17) is FT-ISS with respect to $\boldsymbol{\xi}$. The trajectories satisfies

$$\begin{aligned}&||\tilde{\vartheta}\left(t,\tilde{\vartheta}_0\right)|| \leqslant \\ &\sqrt{c_1}\left(c_2^{\frac{\alpha-1}{2}}||\tilde{\vartheta}_0||^{1-\alpha} + \frac{\sigma_1(1-\zeta)(1-\alpha)\varrho_{\min}^{\alpha+1}c_2^{\frac{\alpha+1}{2}}}{2}t\right)^{\frac{1}{1-\alpha}} \\ &\forall t \leqslant T_{\tilde{\vartheta}_1}\end{aligned} \tag{18a}$$

$$||\tilde{\vartheta}\left(t,\tilde{\vartheta}_0\right)|| \leqslant \sqrt{\frac{c_1}{c_2}}\mu_{\tilde{\vartheta}_1}||\boldsymbol{\xi}||_\infty \quad \forall t > T_{\tilde{\vartheta}_1} \tag{18b}$$

where $\tilde{\vartheta}_0 = \tilde{\vartheta}(0), c_1 = 2\lambda_{\max}(\boldsymbol{\tau}), c_2 = 2\lambda_{\min}(\boldsymbol{\tau}), \sigma_1\in(0,1)$, and

$$\mu_{\tilde{\vartheta}_1} = \frac{(2\sigma_2)^{\frac{1}{\alpha+1}}||\boldsymbol{CT}^{-1}||}{(\zeta\sigma_1)^{\frac{1}{\alpha+1}}\varrho_{\min}}$$

$$T_{\tilde{\vartheta}_1} \leqslant \max\left[0 \quad \frac{2\left(c_2^{\frac{\alpha-1}{2}}||\tilde{\vartheta}_0||^{1-\alpha} - c_1^{\frac{\alpha-1}{2}}\mu_{\tilde{\vartheta}_1}^{1-\alpha}\right)}{\sigma_1(1-\zeta)(1-\alpha)\varrho_{\min}^{\alpha+1}c_2^{\frac{\alpha+1}{2}}}\right]$$

for any $\tilde{\vartheta}_0\in\mathbb{R}, \zeta\in(0,1)$ and $\sigma_2 = \max\left(\sigma_1+1, \frac{\sigma_1}{(1-\sigma_1^{\frac{1}{\alpha}})\alpha}\right)$.

Then for the parameter updating law (8b), consider the Lyapunov function

$$V_{\tilde{\omega}} = \frac{1}{2}\tilde{\omega}^T\boldsymbol{\tau}^{-1}\tilde{\omega} \tag{19}$$

satisfying

$$c_1^{-1}||\tilde{\omega}||^2 \leqslant V_{\tilde{\omega}}(\tilde{\omega}) \leqslant c_2^{-1}||\tilde{\omega}||^2 \tag{20a}$$

$$c_1^{-\frac{\alpha+1}{2}}||\tilde{\omega}||^{\alpha+1} \leqslant V_{\tilde{\omega}}^{\frac{\alpha+1}{2}}(\tilde{\omega}) \leqslant c_2^{-\frac{\alpha+1}{2}}||\tilde{\omega}||^{\alpha+1}. \tag{20b}$$

Next, as outlined in process [23], if $\alpha \in (0,1)$, the derivative of $V_{\tilde{\omega}}$ along the trajectory of dynamic (17), yields

$$pV_{\tilde{\omega}}(\tilde{\omega}) \leqslant -\sigma_1(1-\zeta)\varrho_{\min}^{\alpha+1}c_2^{\frac{\alpha+1}{2}}V_{\tilde{\omega}}^{\frac{\alpha+1}{2}} \tag{21a}$$

$$\forall||\tilde{\omega}|| \geqslant \frac{(2\sigma_2)^{\frac{1}{\alpha+1}}||\boldsymbol{CT}^{-1}||}{(\zeta\sigma_1)^{\frac{1}{\alpha+1}}\varrho_{\min}}||\boldsymbol{\xi}||_\infty \tag{21b}$$

for any $\zeta \in (0,1)$, which suggests (17) is FT-ISS with respect to $\boldsymbol{\xi}$.

If $\alpha = 0$, we have the following lemma.

Lemma 2 (See [24]): If $0 < \varrho_{\min} < \epsilon_{\min}(\boldsymbol{C\Omega}(t))$ for all $t > 0$ and $||\boldsymbol{C\Omega}||_\infty < \varrho_{\max} < +\infty$. Then, for $\alpha = 0$, the dynamic (17) is FT-ISS with respect to $\boldsymbol{\xi}$. The trajectories satisfies

$$||\tilde{\vartheta}\left(t,\tilde{\vartheta}_0\right)|| \leqslant \tag{22a}$$

$$\sqrt{c_1}\left(c_2^{-\frac{1}{2}}||\tilde{\vartheta}_0|| + \frac{\sigma_1(1-\zeta)\varrho_{\min}c_2^{\frac{1}{2}}}{2}t\right) \quad \forall t \leqslant T_{\tilde{\vartheta}_1} \tag{22b}$$

$$||\tilde{\vartheta}\left(t,\tilde{\vartheta}_0\right)|| \leqslant \sqrt{\frac{c_1}{c_2}}\mu_{\tilde{\vartheta}_2}||\boldsymbol{\xi}||_\infty \quad \forall t > T_{\tilde{\vartheta}_2} \tag{22c}$$

where

$$\mu_{\tilde{\vartheta}_2} = \frac{2\sigma_2||\boldsymbol{CT}^{-1}||}{\zeta\sigma_1\varrho_{\min}}$$

$$T_{\tilde{\vartheta}_2} \leqslant \max\left[0 \quad \frac{2\left(c_2^{-\frac{1}{2}}||\tilde{\vartheta}_0|| - c_1^{-\frac{1}{2}}\mu_{\tilde{\vartheta}_2}\right)}{\sigma_1(1-\zeta)\varrho_{\min}c_2^{\frac{1}{2}}}\right]$$

for any $\tilde{\vartheta}_0 \in \mathbb{R}, \zeta \in (0,1)$, and $\sigma_2 > \sigma_1 + 1$.

Then recalling the Lyapunov function (19), if $\alpha = 0$, the derivative of $V_{\tilde{\omega}}$ along the trajectory of dynamic (17), yields

$$pV_{\tilde{\omega}}(\tilde{\omega}) \leqslant -\sigma_1(1-\zeta)\varrho_{\min}c_2^{\frac{1}{2}}V_{\tilde{\omega}}^{\frac{1}{2}} \tag{23a}$$

$$\forall||\tilde{\omega}|| \geqslant \frac{2\sigma_2||\boldsymbol{CT}^{-1}||}{\zeta\sigma_1\varrho_{\min}}||\boldsymbol{\xi}||_\infty \tag{23b}$$

for any $\zeta \in (0,1)$, which suggests (17) is FT-ISS with respect to $\boldsymbol{\xi}$.

2) High Order Nonlinear States Observer: In order to conduct the following analysis, we introduce the following lemma.

Lemma 3 (See [25]): Applying observer (8c)–(8e) to system (5)–(7). If $||\boldsymbol{x}||_\infty < +\infty, ||\boldsymbol{u}_{\text{in}}||_\infty < +\infty$ and $||\boldsymbol{G}(t,\boldsymbol{y}(t),\boldsymbol{u}_{\text{in}}(t))||_\infty < +\infty$ for all $t > 0$, then there exists some positive constants k_i making the error dynamics

$$p\boldsymbol{\xi} = \boldsymbol{B\xi} + \boldsymbol{TDw} - \boldsymbol{\chi}\left(\boldsymbol{\xi}_1, \boldsymbol{C\Omega}\tilde{\vartheta}\right) \tag{24}$$

is FT-ISS with respect to the input $\tilde{\vartheta}$. Besides, as reported in [25], if $||\max\{w_\alpha, w_\beta\}||_\infty \leqslant \bar{w}$, then $\boldsymbol{\xi}$ satisfying

$$||\boldsymbol{\xi}(t,\boldsymbol{\xi}_0)|| \leqslant \varsigma_1\varrho_{\max}||\tilde{\omega}||_\infty + \varsigma_2|\boldsymbol{CAD}\bar{w}|^{\frac{1}{2}}\varrho_{\max}^{\frac{1}{2}}||\tilde{\omega}||_\infty^{\frac{1}{2}} \tag{25}$$

for all $t \geqslant T_\xi > 0$ and $\varsigma_i \geqslant 1$ depend only on k_i.

Recalling the input $\boldsymbol{\delta} = \boldsymbol{x} - \boldsymbol{\gamma} + \boldsymbol{\Omega}\tilde{\omega}$, the dynamic of which yields

$$p\boldsymbol{\delta} = (\boldsymbol{A} - \boldsymbol{LC})\boldsymbol{\delta} + \boldsymbol{Dw}(t) \tag{26a}$$

$$\boldsymbol{y}_\delta = \boldsymbol{y} - \boldsymbol{C\gamma} = \boldsymbol{C\delta} - \boldsymbol{C\Omega}\tilde{\omega} \tag{26b}$$

where $\boldsymbol{y}_\delta$ is measurable. Then, conducting transformation $\boldsymbol{\delta}_{\bar{T}} = \boldsymbol{T\delta}$ to (26) we have

$$p\boldsymbol{\delta}_{\bar{T}} = \boldsymbol{B\delta}_{\bar{T}} + \boldsymbol{aCT}^{-1}\boldsymbol{\delta}_{\bar{T}} - \boldsymbol{aC\Omega}\tilde{\omega} + \boldsymbol{TDw} \tag{27a}$$

$$\boldsymbol{y}_\delta = \boldsymbol{CT}^{-1}\boldsymbol{\delta}_{\bar{T}} - \boldsymbol{C\Omega}\tilde{\omega}. \tag{27b}$$

Then, design observer (8e) for (27), the error dynamics for $\boldsymbol{\xi} = \boldsymbol{\delta}_{\bar{T}} - \boldsymbol{\eta}$ yields

$$p\boldsymbol{\xi} = \boldsymbol{B\xi} + \boldsymbol{TDw} - \boldsymbol{\chi}(\boldsymbol{\eta}_1, \boldsymbol{y} - \boldsymbol{C\gamma}). \tag{28}$$

It is note worthy that $\boldsymbol{y} - \boldsymbol{C\gamma} - \boldsymbol{\eta}_1 = \boldsymbol{CT}^{-1}\boldsymbol{\delta}_{\bar{T}} - \boldsymbol{C\Omega}\tilde{\omega} - \boldsymbol{\eta}_1$ and the correction term $\boldsymbol{\chi}_1$ is given by

$$\boldsymbol{\chi}_1(\boldsymbol{\xi}_1, \boldsymbol{C\Omega}\tilde{\omega}) = \begin{bmatrix} k_1\langle\boldsymbol{\xi}_1 - \boldsymbol{C\Omega}\tilde{\omega}\rangle^{\frac{1}{2}} \\ k_2\langle\boldsymbol{\xi}_1 - \boldsymbol{C\Omega}\tilde{\omega}\rangle^0 \end{bmatrix} \tag{29}$$

where $\boldsymbol{\xi}_1 = \boldsymbol{CT}^{-1}\bar{\boldsymbol{\delta}} - \boldsymbol{\eta}_1$. Then, we have

$$p\boldsymbol{\xi} = \boldsymbol{B\xi} + \boldsymbol{TDw} - \boldsymbol{\chi}_1(\boldsymbol{\xi}_1, \boldsymbol{C\Omega}\tilde{\omega}). \tag{30}$$

Then, note that (30) falls into the form of (24). Since we have defined in (8c) that $\hat{\boldsymbol{x}} = \boldsymbol{\gamma} + \boldsymbol{T}^{-1}\boldsymbol{\eta}$, and define $\boldsymbol{\xi} = \boldsymbol{T\delta} - \boldsymbol{\eta}, \boldsymbol{\delta} = \boldsymbol{x} - \boldsymbol{\gamma} + \boldsymbol{\Omega}\tilde{\omega}$, then we have

$$\boldsymbol{x} - \hat{\boldsymbol{x}} = \boldsymbol{T}^{-1}\boldsymbol{\xi} - \boldsymbol{\Omega}\tilde{\omega}. \tag{31}$$

Hence, according to Lemma 3, the state estimation error $\boldsymbol{x} - \hat{\boldsymbol{x}}$ is FT-ISS with respect to $\tilde{\omega}$.

C. Parameter Tuning Guideline

Recalling the adaptive observer (8), the selection of $\boldsymbol{L}$ should insure $(\boldsymbol{A} - \boldsymbol{LC})$ is Hurwitz. $\boldsymbol{L}$ is the gain vector of the high gain observer (8d), according to [26] and [27], the tuning process of $\boldsymbol{L}$ is transformed into tuning bandwidth of the observer. Then, $\boldsymbol{L}$ is recommended as $\boldsymbol{L} = [L_1 \quad L_1 \quad L_2 \quad L_2]^T$ where $L_i, i = 1,2$ satisfying $L_1 = 2\omega_0$ and $L_2 = {\omega_0}^2$, where $\omega_0 > 0$ is the bandwidth of the high gain observer.

The nonlinear characteristic constant α is recommended as 0.5 to balance the chattering and dynamic performance. Specific explanations will be provided in the next section.

According to the findings presented in [25], if for some known positive constant $\bar{w}$ satisfying $||\max\{w_\alpha, w_\beta\}||_\infty \leqslant \bar{w}$, then the gains $k_i, i = 1,2$ are recommended as $k_1 = 1.5|\boldsymbol{CAD}\bar{w}|^{0.5}$ and $k_2 = 1.1|\boldsymbol{CD}\bar{w}|$, respectively.

Up to now, the entire design process is complete, and the inputs of the adaptive observer are voltage $\boldsymbol{u}$ and current $\boldsymbol{i}$, while the outputs are the estimated speed $\hat{\omega}$ and the states $\hat{\boldsymbol{\psi}}_\mu$ and $\hat{\boldsymbol{\varpi}}_\psi$. Based on the estimated speed-flux production $\hat{\boldsymbol{\varpi}}_\psi$, reverting $\hat{\boldsymbol{\varpi}}_\psi$ back to the active flux linkage $\hat{\boldsymbol{\psi}}_a$, then the estimated rotor position $\hat{\theta}$ can be obtained as

$$\hat{\theta} = \arctan\left(\frac{\hat{\varpi}_{\psi\alpha}}{\hat{\omega}} - L_q i_\beta, -\frac{\hat{\varpi}_{\psi\beta}}{\hat{\omega}} - L_q i_\alpha\right). \tag{32}$$

Accordingly, based on the designed HONA observer, the sensorless drive system is constructed as shown in Fig. 4.

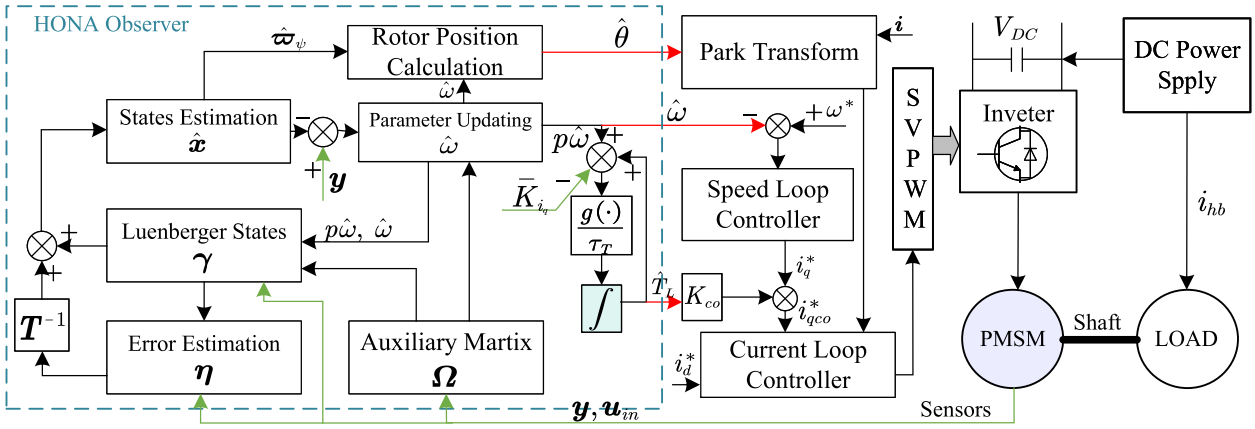

Fig. 4. PMSM sensorless drive system with proposed observation scheme.

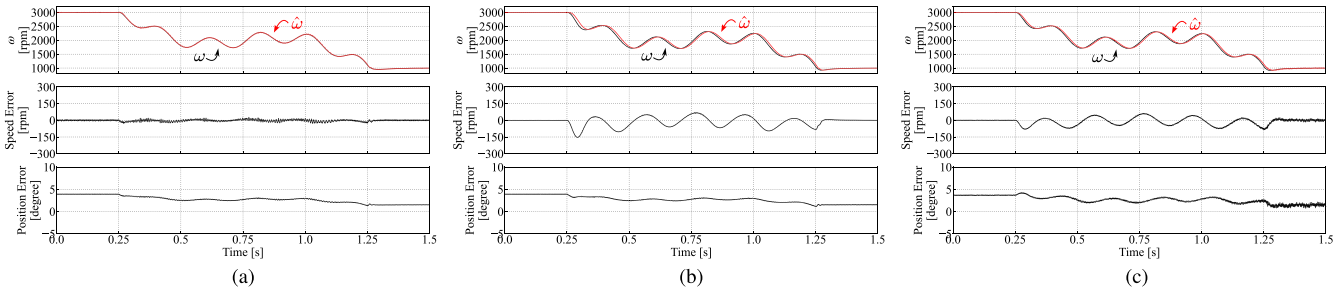

Fig. 5. Sensorless dynamic performance test with $\omega^* = -2000t - 500\sin(\pi t) - 200\sin(5\pi t), t \in (0.25, 1.25)$. (a) HONA observer with $\alpha = 0.5$. (b) HONA observer with $\alpha = 1$. (c) Conventional high order SMO.

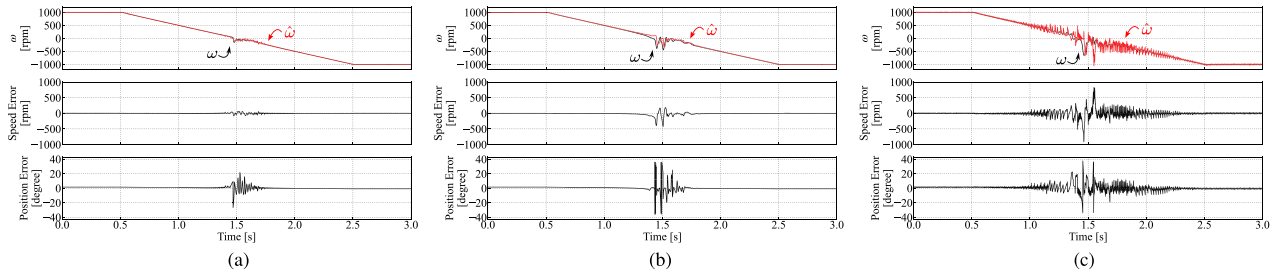

Fig. 6. Sensorless slow speed reversal test with slope of -1000 r/min/s. (a) HONA observer with $\alpha = 0.5$. (b) HONA observer with $\alpha = 1$. (c) Conventional high order SMO.

IV. Numerical Results

This section arranges a series of comparative numerical simulation tests to validate the performance of the proposed observer. The numerical integration method chosen is the well-known fourth order Runge-Kutta method. The simulated motor prototype has nameplate values of 2.4 Nm, 0.75 kW, and 3000 r/min. Other parameters are provided in the following table.

Fig. 5 presents a comparative dynamic performance testing of the proposed observer under sensorless operating conditions with $\alpha = 0.5$ and $\alpha = 1$. The speed reference is set to $\omega^* = 3000, t \in [0, 0.25], \omega^* = -2000t - 500\sin(\pi t) - 200\sin(5\pi t), t \in (0.25, 1.25), \omega^* = 1000$, and $t \in [1.25, 1.5]$. The figure indicates that the proposed HONA observer exhibits satisfying dynamic performance when $\alpha = 0.5$, and compared to the conventional high order SMO mentioned in [28], there is no significant performance degradation as the speed decreases.

Fig. 6 further compares the performance during slow reversal with a slope of -1000 r/min/s. It can be observed that the conventional high order SMO struggles to maintain stability as the speed approaches zero, with performance rapidly deteriorating. In contrast, the proposed observer maintains relatively good convergence at low speeds. Particularly when $\alpha = 0.5$, the estimation error is small, and the dynamic performance is satisfactory.

Fig. 7 analyzes the antidisturbance performance of the proposed HONA observer. In this analysis, the speed is maintained at 3000 r/min, and a load torque defined as $T_L = \sin(5\pi t)$,

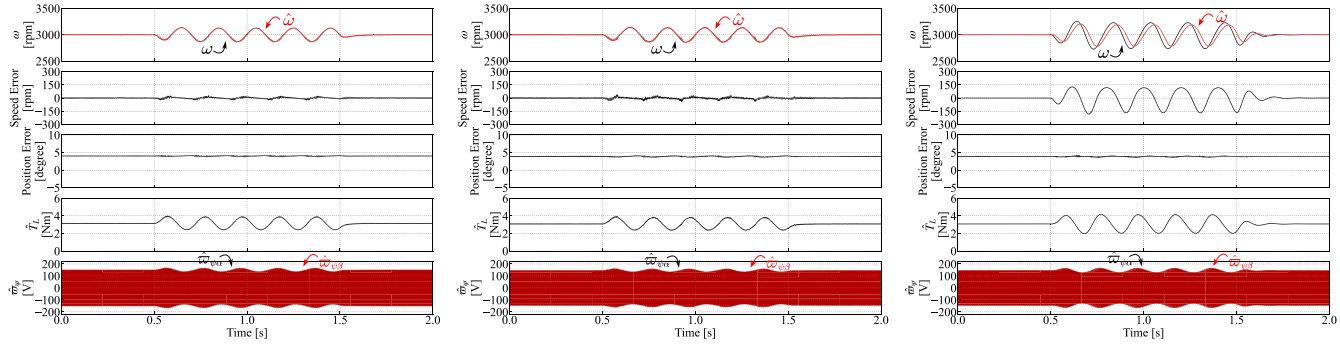

Fig. 7. HONA observer antidisturbance test with $T_L = \sin(5\pi t), t \in (0.5, 1.5)$. (a) $\alpha = 0.5$ with load torque compensation. (b) $\alpha = 0.5$ without load torque compensation. (c) $\alpha = 1$ without load torque compensation.

TABLE I
PARAMETERS OF PMSM PROTOTYPE

Item	Notation	Value
Pole pairs	n_{pp}	5
Stator resistance	R_s	2.292 Ω
d-axis inductance	L_d	8.26 mH
q-axis inductance	L_q	11.54 mH
Flux	ψ_f	0.07 Wb
Moment of inertia	J_s	0.00115 kg · m^2

is applied for $t \in (0.25, 1.25)$. The figure illustrates that when $\alpha = 0.5$, the observer exhibits superior dynamic performance, with the speed estimation error remaining within 30 r/min, and the speed fluctuation is also smaller compared to when $\alpha = 1$. As shown in Fig. 7(a), with the inclusion of load torque feedforward compensation, the speed fluctuation is further reduced, and the speed estimation error is suppressed, thereby enhancing the system's dynamic performance.

V. EXPERIMENTAL WORKS

A. Experimental Setup

In this section, a series of experiments were conducted to validate the effectiveness of the proposed observer. The parameters of the PMSM used in the experiments are consistent with those in the simulation (listed in Table I). Fig. 8 provides a photograph of the experimental setup, which mainly composed of the controlled PMSM and a hysteresis brake to generate load torque, a TMS320F28335 DSP control board, an inverter, two dc power supplies for dc bus voltage and loading, respectively, and an oscilloscope. The PMSM is driven by the inverter, while the hysteresis brake generates a load torque opposing the direction of the PMSM's motion, with representation as $-\mathcal{L}_{\text{dc}} i_{hb} \text{sign}(\omega)$, where $\mathcal{L}_{\text{dc}}$ is the torque coefficient and i_{hb} is the current inputted into hysteresis brake. During the experiments, the actual speed and angle are measured by a 2500-ppr encoder for analysis. The bandwidths of the speed loop and current loop controllers are

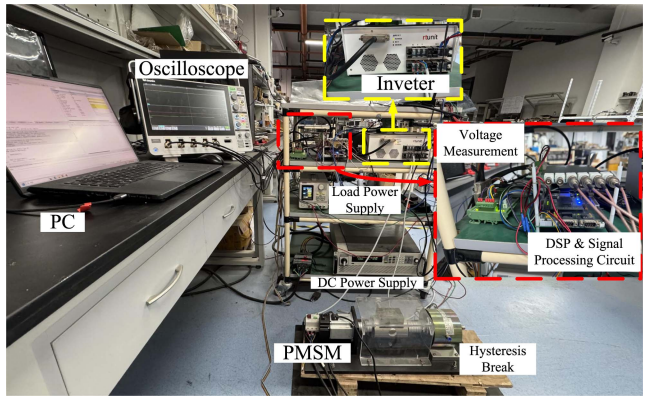

Fig. 8. Experimental platform.

set to 50 and 250 Hz, respectively. The improved Euler method is employed during the discretization process. Following the tuning guideline in Section III-C, the parameters of the observer are chosen as $\omega_0 = 800$ and $\bar{w} = 1600$. The conventional high order SMO for comparison is the one mentioned in [28], with the lower order gain set to 120 and the higher order gain set to 5000.

B. Experimental Results

Fig. 9 presents a continuous dynamic performance comparison test. The motor operates at 3000 r/min until 3 s, after which the speed reference decreases with a slope of −900 r/min/s for 3 s, then immediately increases at 900 r/min/s for 3 s, forming one complete cycle. After the second cycle, the speed returns to 3000 r/min. This implies that during the 3 ∼ 15 s interval, the motor undergoes a continuous dynamic process with the minimum speed reference reaching 300 r/min.

From Fig. 9, it can be observed that the HONA observer demonstrates satisfactory dynamic performance when $\alpha = 0.5$. In contrast, when $\alpha = 1$, indicating a linear observer, it fails to accurately track the actual speed when the speed reaching lowest point. Although the conventional high-order SMO also shows commendable dynamic performance, it exhibits more

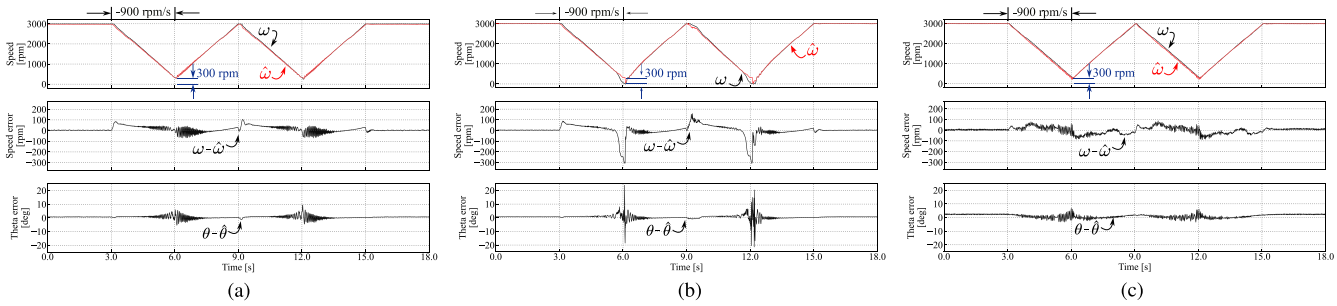

Fig. 9. Experimental sensorless continuous dynamic performance test. (a) HONA observer with $\alpha = 0.5$. (b) HONA observer with $\alpha = 1$. (c) Conventional high order SMO.

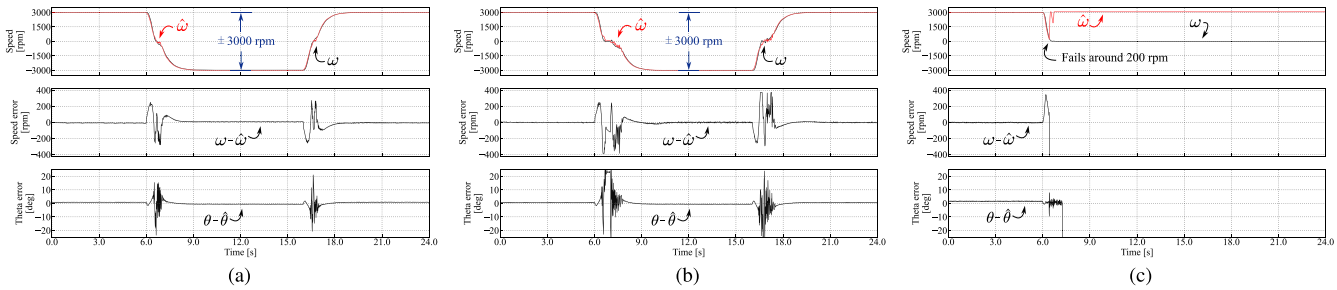

Fig. 10. Experimental sensorless ± 3000 r/min (1.0 p.u. ∼ −1.0 p.u.) fast reversal test. (a) HONA observer with $\alpha = 0.5$. (b) HONA observer with $\alpha = 1$. (c) Conventional high order SMO.

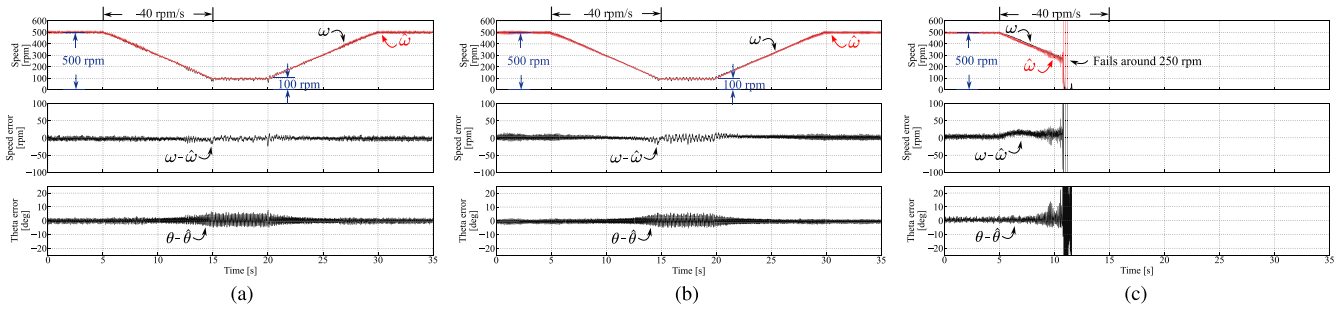

Fig. 11. Experimental sensorless low speed operation test. (a) HONA observer with $\alpha = 0.5$. (b) HONA observer with $\alpha = 1$. (c) Conventional high order SMO.

severe chattering, particularly as the speed decreases, with its performance deteriorating rapidly.

Fig. 10 presents a set of fast ± 3000 r/min (1.0 p.u. ∼ −1.0 p.u.) reversal experiments. The speed reference steps from 3000 to −3000 r/min at 3 s and then steps back to 3000 r/min at 16 s. Notably, for conventional high order SMO, due to inherent limitations of the traditional PMSM model, it becomes challenging to maintain stability as the speed approaches zero [5], [29], leading to out of synchronization near 200 r/min. Conversely, the HONA observer demonstrates polished dynamic performance during reversal process. Particularly, when $\alpha = 0.5$, both speed and angle transient errors are optimized as the speed approaches zero.

Fig. 11 presents a set of sensorless low-speed operation experiments. The motor sensorless operates at 500 r/min under rated loaded, decelerating to 100 r/min at a rate of −40 r/min/s at 5 s, and then accelerating back to 500 r/min at 40 r/min/s at 20 s. As shown in the figure, the conventional high order SMO loses stability when the speed decreases to approximately 250 r/min, whereas the HONA observer remains stable even at 100 r/min (0.03 p.u.). It can be observed that when $\alpha = 0.5$, although the inherent characteristics of the nonlinear parameter updating law introduce some chattering, the dynamic performance and stability at low-speed steady-state operation are improved compared to $\alpha = 1$.

The test shown in Fig. 12 was designed to compare the load carrying capabilities of the proposed HONA observer under varying degrees of linearity and with or without feedforward compensation. The motor speed reference steps from 500 to 1500 r/min at 2 s, followed by a sudden 1 Nm load. At the

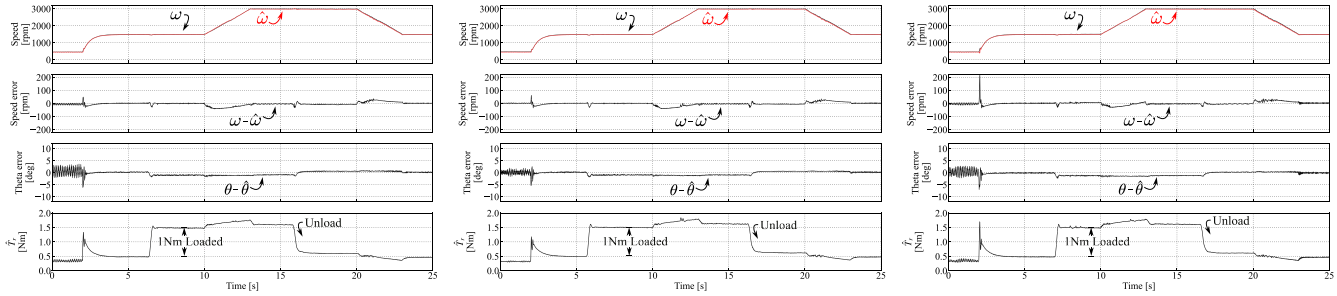

Fig. 12. Experimental sensorless dynamic test for HONA observer. (a) $\alpha = 0.5$ with load torque compensation. (b) $\alpha = 0.5$ without load torque compensation. (c) $\alpha = 1$ without load torque compensation.

10 and 20 s, the speed is increased and decreased by 500 r/min/s for 3 s, respectively, and the load is removed during the period when the speed reaches 3000 r/min.

Fig. 12(a) and (b) show that load feedforward compensation causes a certain degree of steady-state angle error oscillation at low speeds due to the inherent oscillation in load estimation at these speeds. However, during the loaded continuous dynamic phase (10∼13 s), the speed dynamic performance is improved. Simultaneously, it enhances dynamic performance during step acceleration and loading. Furthermore, (b) and (c) illustrate that dynamic performance is superior when $\alpha = 0.5$ compared to $\alpha = 1$, which is particularly evident during the speed step change at 2 s.

VI. Conclusion

This article addresses the challenge of constructing a speed adaptive observer in traditional models by the speed-flux transformation through the active flux model of PMSM, thereby constructing a speed-flux model with a known regression term. This model achieves known regression term by applying nonlinear parameterization to the motor speed. On this basis, a HONA observer is developed, enhancing dynamic performance by designing the parameter update law as nonlinear while the correction term for the error estimation dynamics is designed in the form of a high order sliding mode. Besides, the known speed regression term feature of the speed-flux transformation model ensures stability over a wide speed range. Numerical and experimental results demonstrate that the HONA observer offers advantages in low-speed range and dynamic performance compared to linear and conventional high order SMO during continuous dynamic processes, reversal and low speed scenarios.

References

[1] J. Chen, X. Yuan, F. Blaabjerg, and C. H. T. Lee, "Overview of fundamental frequency sensorless algorithms for AC motors: A unified perspective," *IEEE Trans. Emerg. Sel. Topics Power Electron.*, vol. 11, no. 1, pp. 915–931, Feb. 2023.

[2] Z. Chen, M. Tomita, S. Doki, and S. Okuma, "An extended electromotive force model for sensorless control of interior permanent-magnet synchronous motors," *IEEE Trans. Ind. Electron.*, vol. 50, no. 2, pp. 288–295, Apr. 2003.

[3] I. Boldea, M. C. Paicu, and G.-D. Andreescu, "Active flux concept for motion-sensorless unified AC drives," *IEEE Trans. Power Electron.*, vol. 23, no. 5, pp. 2612–2618, Sep. 2008.

[4] C. J. Volpato Filho and R. P. Vieira, "Adaptive full-order observer analysis and design for sensorless interior permanent magnet synchronous motors drives," *IEEE Trans. Ind. Electron.*, vol. 68, no. 8, pp. 6527–6536, Aug. 2021.

[5] Y. Zuo, C. Lai, and K. L. V. Iyer, "A review of sliding mode observer based sensorless control methods for PMSM drive," *IEEE Trans. Power Electron.*, vol. 38, no. 9, pp. 11352–11367, Sep. 2023.

[6] L. Zheng, C. Wu, F. Shentu, and C. Wu, "An accurate full-speed position estimation for permanent magnet synchronous motors with a DC-bus current sensor," *IEEE Trans. Power Electron.*, vol. 39, no. 9, pp. 11468–11478, Sep. 2024.

[7] D. Jin and L. Liu, "Adaptive second-order disturbance observer-based position sensorless drive strategy for PMSM," *IEEE Trans. Power Electron.*, vol. 39, no. 12, pp. 16415–16428, Dec. 2024.

[8] J. Chen and J. Huang, "Application of adaptive observer to sensorless induction motor via parameter-dependent transformation," *IEEE Trans. Control Syst. Technol.*, vol. 27, no. 6, pp. 2630–2637, Nov. 2019.

[9] Q. Lin, L. Liu, and D. Liang, "Adaptive observer design for sensorless IPMSM drives with known regressors variant of extended EMF model," *IEEE Trans. Power Electron.*, vol. 39, no. 1, pp. 212–224, Jan. 2024.

[10] Q. Lin, L. Liu, D. Liang, D. Jin, S. Jia, and H. Song, "A dual-level adaptive law design for super-twisting algorithm in sensorless IPMSM drives," *IEEE Trans. Ind. Appl.*, vol. 59, no. 5, pp. 5945–5956, Sep./Oct. 2023.

[11] D. Liang, J. Li, R. Qu, and W. Kong, "Adaptive second-order sliding-mode observer for PMSM sensorless control considering VSI nonlinearity," *IEEE Trans. Power Electron.*, vol. 33, no. 10, pp. 8994–9004, Oct. 2018.

[12] J. Chen, J. Huang, and Y. Sun, "Resistances and speed estimation in sensorless induction motor drives using a model with known regressors," *IEEE Trans. Ind. Electron.*, vol. 66, no. 4, pp. 2659–2667, Apr. 2019.

[13] M. Farza, M. M'Saad, T. Maatoug, and M. Kamoun, "Adaptive observers for nonlinearly parameterized class of nonlinear systems," *Automatica*, vol. 45, no. 10, pp. 2292–2299, 2009. [Online]. Available: https://www.sciencedirect.com/science/article/pii/S0005109809002994

[14] I. Y. Tyukin, E. Steur, H. Nijmeijer, and C. van Leeuwen, "Adaptive observers and parameter estimation for a class of systems nonlinear in the parameters," *Automatica*, vol. 49, no. 8, pp. 2409–2423, 2013. [Online]. Available: https://www.sciencedirect.com/science/article/pii/S0005109813002781

[15] H. K. Khalil and L. Praly, "High-gain observers in nonlinear feedback control," *Int. J. Robust Nonlinear Control*, vol. 24, no. 6, pp. 993–1015, 2014. [Online]. Available: https://onlinelibrary.wiley.com/doi/abs/10.1002/rnc.3051

[16] M. Ran, J. Li, and L. Xie, "A new extended state observer for uncertain nonlinear systems," *Automatica*, vol. 131, 2021, Art. no. 109772. [Online]. Available: https://www.sciencedirect.com/science/article/pii/S0005109821002922

[17] G. Wang, M. Valla, and J. Solsona, "Position sensorless permanent magnet synchronous machine drives—A review," *IEEE Trans. Ind. Electron.*, vol. 67, no. 7, pp. 5830–5842, Jul. 2020.

[18] A. Andersson and T. Thiringer, "Motion sensorless IPMSM control using linear moving horizon estimation with Luenberger observer state feedback," *IEEE Trans. Transport. Electrific.*, vol. 4, no. 2, pp. 464–473, Jun. 2018.

[19] H. Kim, J. Son, and J. Lee, "A high-speed sliding-mode observer for the sensorless speed control of a PMSM," *IEEE Trans. Ind. Electron.*, vol. 58, no. 9, pp. 4069–4077, Sep. 2011.

[20] T. Zhang, Z. Xu, and C. Gerada, "A nonlinear extended state observer for sensorless IPMSM drives with optimized gains," *IEEE Trans Ind Appl*, vol. 56, no. 2, pp. 1485–1494, Mar./Apr. 2020.
[21] S. Liu, L. Liu, Q. Lin, and D. Liang, "Fixed-time high-order dynamic observation strategy for PMSM sensorless control," *IEEE Trans. Power Electron.*, vol. 39, no. 12, pp. 16442–16457, Dec. 2024.
[22] H. Sun, X. Zhang, X. Liu, and H. Su, "Adaptive robust sensorless control for PMSM based on improved back EMF observer and extended state observer," *IEEE Trans. Ind. Electron.*, vol. 71, no. 12, pp. 16635–16643, Dec. 2024.
[23] R. Franco, H. Ríos, D. Efimov, and W. Perruquetti, "Adaptive estimation for uncertain nonlinear systems with measurement noise: A sliding-mode observer approach," *Int. J. Robust Nonlinear Control*, vol. 31, no. 9, pp. 3809–3826, 2021.
[24] H. Ríos, R. Franco, A. F. de Loza, and D. Efimov, "A high-order sliding-mode adaptive observer for uncertain nonlinear systems," *IEEE Trans. Autom. Control*, vol. 68, no. 1, pp. 408–415, Jan. 2023.
[25] A. Levant, "Higher-order sliding modes, differentiation and output-feedback control," *Int. J. Control*, vol. 76, no. 9–10, pp. 924–941, 2003.
[26] J. Yao, Z. Jiao, and D. Ma, "Extended-state-observer-based output feedback nonlinear robust control of hydraulic systems with backstepping," *IEEE Trans. Ind. Electron.*, vol. 61, no. 11, pp. 6285–6293, Nov. 2014.
[27] Z. Gao, "Scaling and bandwidth-parameterization based controller tuning," in *Proc. 2003 Amer. Control Conf.*, 2003, vol. 6, pp. 4989–4996.
[28] Z. Yin, Y. Zhang, X. Cao, D. Yuan, and J. Liu, "Estimated position error suppression using novel PLL for IPMSM sensorless drives based on full-order SMO," *IEEE Trans. Power Electron.*, vol. 37, no. 4, pp. 4463–4474, Apr. 2022.
[29] Q. Lin, L. Liu, and D. Liang, "Hybrid active flux observer to suppress position estimation error for sensorless IPMSM drives," *IEEE Trans Power Electron*, vol. 38, no. 1, pp. 872–886, Jan. 2023.

Siyuan Liu (Graduate Student Member, IEEE) received the B.Sc. degree in electrical engineering from the Huazhong University of Science and Technology, Wuhan, China, in 2021. He is currently working toward the Ph.D. degree in electrical engineering with the School of Electrical Engineering, Xi'an Jiaotong University, Xi'an, China.

His research interests include high order nonlinear observers and its application to electrical machine sensorless drives.

Ling Liu (Member, IEEE) received the B.S. degree in electronic information from Xi'an Polytechnic University, Xi'an, China, in 2003, the M.S.degree in measuring and testing technologies and instruments from Southwest Jiaotong University, Chengdu, China, in 2006, and the Ph.D. degree in electrical engineering from Xi'an Jiaotong University, Xi'an, in 2011.

He is currently a Professor with the School of Electrical Engineering, Xi'an Jiaotong University. He has authored or coauthored several technical papers and industrial reports. His current research interests include electrical machines, control theory and applications, nonlinear systems, and electric vehicle.

Dr. Liu is a Senior Member of China Electrotechnical Society.

Qilian Lin (Student Member, IEEE) received the B.Sc. degree in electrical engineering from Hunan University, Changsha, China, in 2019. He is currently working toward the Ph.D. degree in electrical engineering with the School of Electrical Engineering, Xi'an Jiaotong University, Xi'an, China.

His research interests include parameter identification and sensorless control of electric machines, with a special focus on the speed-adaptive full-order observer design.

Dongsong Jin (Student Member, IEEE) received the B.Sc. degree in electrical engineering from Northeast Electric Power University, Jilin, China, in 2020. He is currently working toward the Ph.D. degree in electrical engineering with the School of Electrical Engineering, Xi'an Jiaotong University, Xi'an, China.

His research interests include sensorless drive of electric machines and disturbance compensation of motor system.

Deliang Liang (Senior Member, IEEE) received the B.S., M.S., and Ph.D. degrees in electrical engineering from Xi'an Jiaotong University, Xi'an, China, in 1989, 1992, and 1996, respectively.

Since 1999, he has been with the School of Electrical Engineering, Xi'an Jiaotong University, where he is currently a Professor. From 2001 to 2002, he was a Visiting Scholar with the Science Solution International Laboratory, Tokyo, Japan. His research interests include optimal design, control, and simulation of electrical machines and electrical machine technology in renewable energy.